

Capillary Temperature Calibration for Raman Spectroscopy

Kesini Chumphuthong (Dai), Thailand

September 10, 2025

Abstract

Accurate temperature control and calibration are essential for reliable measurements in Raman microscopy, particularly when investigating phase transitions of liquids confined in microcapillaries. In this study, a systematic calibration of the Linkam heating stage was performed using four different liquids with well-defined melting points: water, 1-undecane, n-decane, and n-dodecane. Each liquid was confined in square glass capillaries of four inner diameters (100 µm, 200 µm, 500 µm, and 1000 µm). The melting process was characterized by monitoring the onset and completion of melting, from which the average melting temperature was determined and compared with literature values.

The results reveal a systematic deviation between the Linkam readout and the true sample temperature, with the magnitude of the deviation depending on the capillary size. A linear calibration function was established for each capillary diameter, with fitted parameters a and b describing the offset and scaling factor, respectively. These calibration relations provide a correction framework that enables more accurate interpretation of melting behavior in confined liquids.

This work demonstrates that temperature calibration is crucial when using microcapillaries in Raman experiments, as confinement effects and instrumental offsets can significantly influence the apparent melting temperature. The developed calibration procedure offers a practical approach for improving the accuracy of future Raman microscopy studies involving temperature-dependent phenomena.

1 Introduction

The study of phase transitions in liquids has received significant attention in recent years. While the classical states of matter—solid, liquid, and gas—are well known, recent research has identified additional liquid states, such as supercooled liquids and liquid-liquid transitions, which exhibit unusual and intriguing behaviors. Understanding these anomalous properties provides valuable insight into molecular interactions and material behavior under extreme conditions and can even help explain natural phenomena, such as climate processes.

Precise temperature control is crucial in these studies, as the behavior of liquids is highly sensitive to both temperature and pressure. This is especially important when using advanced probing techniques, such as Raman spectroscopy, which enables detailed analysis of molecular vibrations and rotations.

Several techniques exist to study the properties of liquids, including methods that confine the liquid within capillaries. In this work, I focus on investigating the melting behavior of liquids. A key challenge in such experiments is that the temperature recorded by the instrument may not accurately reflect the actual temperature of the liquid inside the capillary. To address this, temperature calibration is necessary. Accurate calibration ensures that the temperature readout from the Raman microscope closely corresponds to the true temperature of the sample, which is essential for correctly interpreting the Raman spectra and obtaining reliable insights into the behavior of liquids confined within capillaries. » start focus on water: see the anomalous behavior

2 Theory

2.1 Phase Transitions

As macroscopic variables such as temperature or pressure are varied, the physical state of a system can undergo abrupt and often dramatic changes. These changes are known as phase transitions. Common examples include the transition from solid to liquid (melting) and from liquid to gas (vaporization). Such transformations are fundamental in thermodynamics and statistical physics, as they illustrate how microscopic interactions give rise to macroscopic phenomena.

A phase transition occurs when one phase becomes more thermodynamically stable than another. In equilibrium, the stable phase is the one with the lowest Gibbs free energy, and therefore, any variable that influences free energy—such as temperature, pressure, or composition—can also determine the phase of the system.

Water provides a familiar and illustrative example. Depending on the conditions, it can exist in solid (ice), liquid, or gaseous (steam) phases. At the molecular level, these phases differ markedly in the degree of order, density, and mobility of the molecules. For instance, ice has a rigid hydrogen-bonded lattice, liquid water has a fluctuating but partially ordered structure, and steam consists of widely separated molecules with minimal intermolecular interactions.

The boundaries between phases are conveniently represented in a phase diagram, which maps the regions of stability of each phase as a function of temperature and pressure as shown in Fig. 1. Although the real phase diagram of water is much more complex—with numerous distinct crystalline ice phases—this simplified representation highlights the essential features relevant to most conditions. It includes the familiar melting, boiling, and sublimation curves, as well as the triple point, where solid, liquid, and vapor coexist, and the critical point, beyond which the distinction between liquid and vapor disappears.

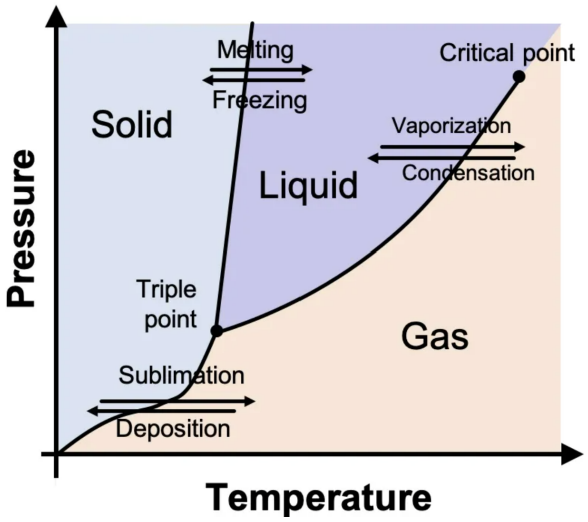


Figure 1: Schematic phase diagram of water, showing the stable regions of solid, liquid, and vapor as functions of temperature and pressure. Key features include the triple point and critical point [1]

2.2 Anomalous Behavior in Water

Water is often described as the most anomalous liquid, displaying a wide range of unusual thermodynamic and structural properties. Among its best-known anomalies are the density maximum at 4 °C, the increase in compressibility and heat capacity upon supercooling, and the unusual pressure dependence of its melting point. These properties set water apart from most other liquids and have profound implications for both natural and technological processes.

At the molecular level, these anomalies arise from the dynamic hydrogen-bond network that characterizes liquid water. Rather than forming a uniform structure, water molecules fluctuate between two distinct local configurations: a high-density liquid (HDL), with a more compact, disordered arrangement, and a low-density liquid (LDL), with an open, tetrahedral network resembling ice. The balance between these two motifs shifts with changes in temperature and pressure, leading directly to water's anomalous macroscopic properties.

This two-state model also predicts the possibility of a liquid–liquid phase transition in deeply supercooled water, ending in a second critical point (see Fig. 2). Although this region is experimentally difficult to access, theoretical and computational studies provide strong evidence for its existence. Such a transition offers a unifying explanation for the pronounced fluctuations in density, heat capacity, and compressibility observed in supercooled water [2].

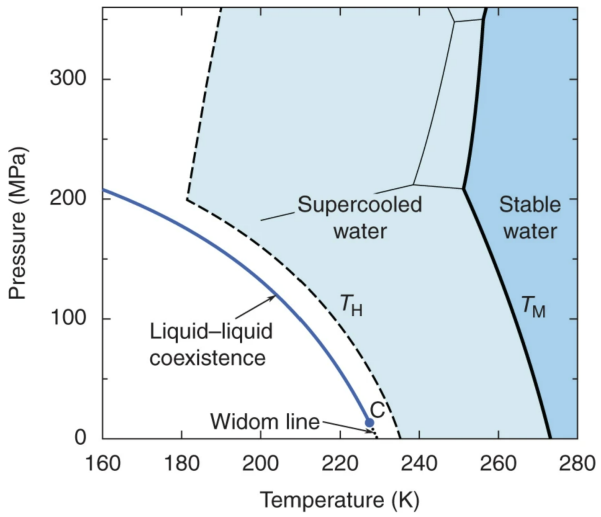


Figure 2: Hypothetical phase diagram of cold water [3].

2.3 Melting Point

The melting point of a substance is the temperature at which a solid becomes a liquid. In reality, most substances do not melt at a single temperature but rather over a melting point range. This range represents the temperatures between when the first crystal begins to melt and when the entire sample becomes liquid.

Several factors can influence the melting point range. Purity plays a major role: impurities disrupt the orderly lattice structure of a solid, often lowering the melting point and broadening the melting range. Experimental conditions, such as the rate of heating, can also affect the observed melting behavior. A rapid heating rate may cause the measured melting point to appear higher or less precise, while slow, controlled heating allows the transition to be observed more accurately ref: [4].

The melting point of a substance is the temperature at which it transitions from solid to liquid. In practice, most substances do not melt at a single temperature but over a *melting point range*. Factors such as purity and heating rate can influence this range. Table 1 shows the melting points of several example substances based on NIST data, along with a qualitative description of the sharpness of their melting points. This highlights how different substances can exhibit sharp or broad melting behaviors depending on their molecular structure and purity.

Table 1: Melting points of example substances from NIST data.

Substance	Melting Point (°C)	Sharpness of Melting Point
Pure water	0.0	Very sharp
1-Undecene	-49.4	Moderate
n-Decane	-29.7	Sharp
n-Dodecane	-9.6	Very sharp
n-Undecane	-26.0	Sharp
2-Propanol (Isopropanol)	-89.5	Sharp
Dimethyl sulfoxide (DMSO)	18.5	Sharp

2.3.1 Melting Point Analysis

The apparent specific heat of n-dodecane can be plotted as a function of temperature at a heating rate of $\beta = 1/600\,\mathrm{K\,s^{-1}}$. The measurement begins with the substance in the solid phase, and the temperature gradually increases until the *premelting state* is reached. Analysis of the resulting melting peak allows determination of several key temperatures: the *onset temperature* (T_{onset}), where the first signs of melting are observed; the *peak temperature* (T_{peak}), corresponding to the maximum heat flow; and the *end of melting temperature* (T_{eom}), where the last solid fraction has melted and the material transitions fully to the liquid phase.

In practice, two main characteristic temperatures are commonly distinguished in melting studies: the *onset temperature*, marking the beginning of melting, and the *endset temperature*, indicating the completion of melting. These temperatures can be used to calculate an average melting temperature, providing a representative value for the melting range. The average temperature in my work is calculated using the equation:

$$T_{\mathrm{avg}} = \frac{T_{\mathrm{onset}} + T_{\mathrm{end}}}{2}. \tag{1}$$

2.4 Raman Spectroscopy

Raman spectroscopy is a vibrational spectroscopic technique used to identify the molecular composition of a sample by analyzing inelastically scattered light. When a laser illuminates a sample, most photons are elastically scattered (Rayleigh scattering) without a change in energy. However, a small fraction of photons interact with molecular vibrations, resulting in energy shifts known as Raman scattering.Raman scattering occurs in two main forms:

- Stokes scattering: the photon loses energy, exciting a molecular vibration.

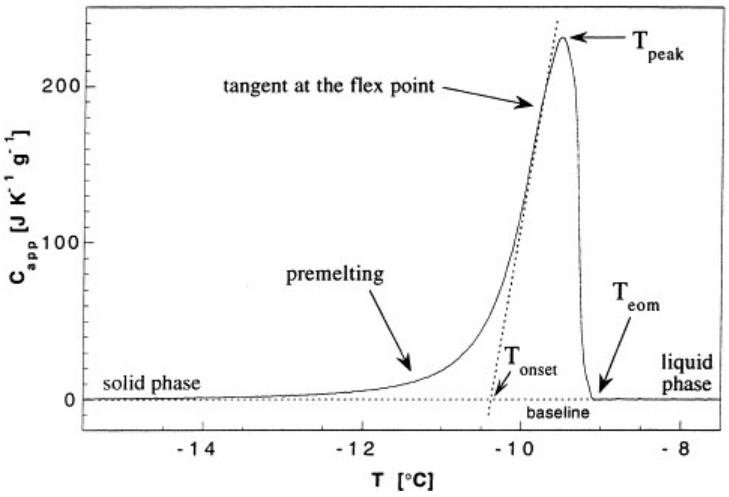


Figure 3: The apparent of a melting curve of n-dodecane, showing the onset, premelting region, and full melting range ref: [5].

- Anti-Stokes scattering: the photon gains energy from a vibrationally excited molecule (typically weaker at room temperature). That is shown in Figure 5

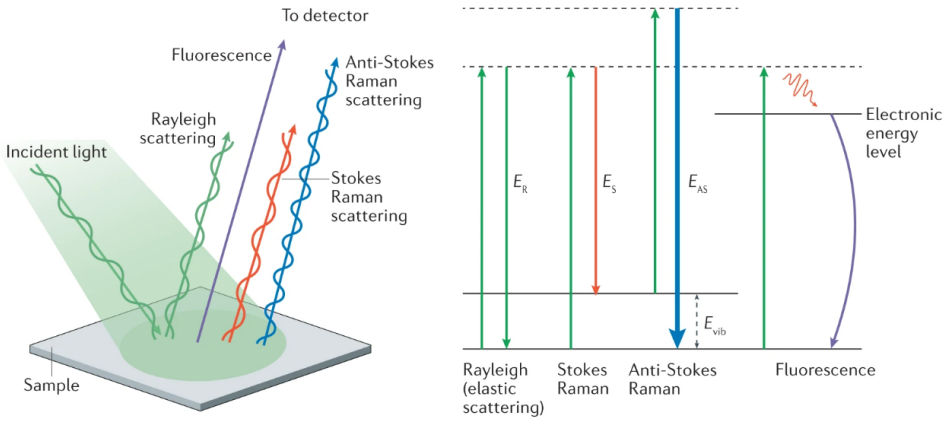


Figure 4: Schematic representation of Stokes and anti-Stokes Raman scattering. The incident photon interacts with a molecule, leading to energy loss (Stokes) or gain (Anti-Stokes).

These shifts in photon energy, expressed in wavenumbers (cm^{-1}), provide a molecular "fingerprint" of the sample, enabling identification of chemical species and monitoring of structural or environmental changes. Raman spectroscopy is particularly useful because it is non-destructive, requires minimal sample preparation, and can probe samples through transparent or thin materials.

Raman spectroscopy complements infrared (IR) spectroscopy. Vibrational modes that change molecular polarizability produce strong Raman signals, while modes that change dipole moment are stronger in IR spectroscopy. This complementarity allows detailed chemical characterization of molecules in a wide variety of materials, including solids, liquids, and biological samples [6].

2.4.1 Raman Spectrometer

A Raman spectrometer is the instrument used to measure Raman scattering and obtain the molecular fingerprint of a sample (see Fig. 5). The basic operation of a Raman spectrometer

begins with a monochromatic laser, which illuminates the sample. The scattered light from the sample contains both Rayleigh scattered light (elastic) and Raman scattered light (inelastic). Only the Raman scattered light is useful for chemical analysis, so filters are used to remove the Rayleigh component before the light enters the rest of the spectrometer.

The Raman scattered light is then separated into its constituent wavelengths using a diffraction grating. When light passes through a grating, different wavelengths are dispersed at slightly different angles. This angular separation allows the spectrometer to measure the precise wavelength shifts associated with molecular vibrations.

After dispersion, the light is detected using a charge-coupled device (CCD) detector. Each wavelength reaches a different position on the detector, creating a spatial map of the Raman scattered light. This information is then processed to generate the Raman spectrum. The choice of laser in Raman spectroscopy is critical and depends on the sample and experimental requirements. Laser power must also be optimized to avoid damaging sensitive samples. The diffraction grating controls the spectral resolution of the measurement. Gratings with higher line densities spread light more, improving spectral resolution but reducing the spectral range captured. Conversely, gratings with lower line densities capture a wider spectral range at lower resolution. Changing the laser wavelength often requires adjustment of the grating to ensure proper separation of Raman scattered light on the detector. Modern spectrometers often feature a grating turret to allow automatic switching of gratings [7].

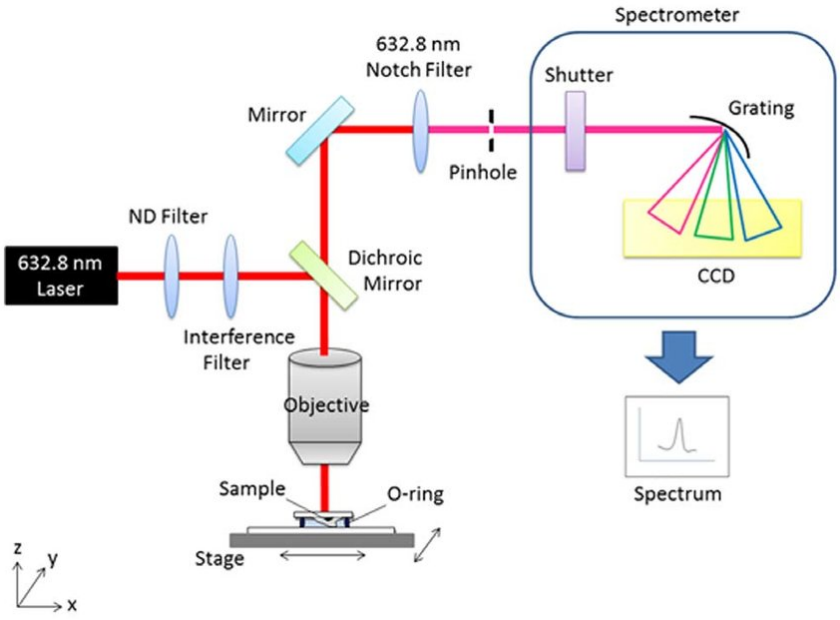


Figure 5: Schematic diagram of the Raman platform set-up [8].

3 Methodology

3.1 Equipments

1. Square Capillaries Square glass capillaries with four different internal diameters were used in the experiments: $100\,\mu m$, $200\,\mu m$, $500\,\mu m$, and $1000\,\mu m$.



Figure 6: Square capillaries of different diameters.

2. Adhesives Two different adhesives were tested for sealing:
   - Norlan Optical Adhesive 81 (UV curing)
   - UHU Plus Schnekkfest

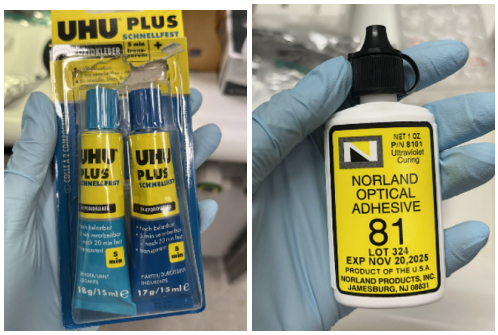


Figure 7: Examples of adhesives: (left) Norlan Optical Adhesive 81 (UV curing), (right) UHU Plus Schnekkfest.

3. Glass Cover Slip
4. Raman Microscope (see Fig. 8)
5. Sample Substances Four different liquids were studied: deionized and degassed water, *n*-decane, 1-undecene, and *n*-dodecane (see Fig. 9).
6. Elmasonic Ultrasonic Bath An Elmasonic ultrasonic bath was used for degassing and cleaning (see Fig. 10).
7. Temperature Controlled Stage The Linkam THMS600/720 temperature-controlled stage was used for heating and cooling experiments (see Fig. 11).

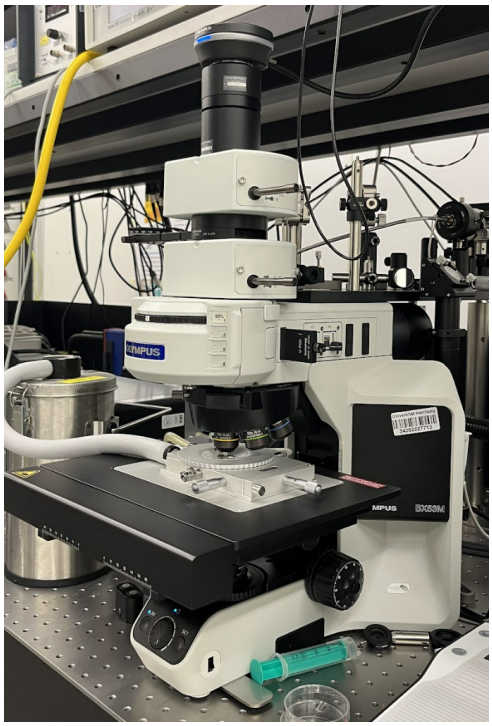


Figure 8: Raman microscope used in the experiment.

3.2 Software and Experiment Setup

3.2.1 Microscope (PRECiV Pro) Setup and Alignment

1. Launch the PRECiV Pro software and calibrate the microscope along the x- and y-axes.
2. Adjust the objective lens to the closest position relative to the stage sample before calibrating the z-axis.
3. Set the illumination mode to transmitted light with an intensity of 50, an exposure time of 300 ms, and a gain of 1.58$\times$.
4. Align the sample under the microscope using reflected light mode.
5. Move the stage horizontally along the x-axis and vertically along the y-axis to position the capillary sample over the aperture of the silver block (temperature-controlled).
6. Adjust the z-axis until the meniscus is sharply focused.

3.2.2 THMS600/720 Temperature-Controlled Stage (Linkam)

1. Place the sample over the aperture of the silver block (temperature-controlled).
2. Ensure that the stage lid is in place and the stage door is closed.
3. Purge the stage using recycled nitrogen gas from the LNP95. Switch on the temperature programmer, set the LNP95 cooling system to maximum speed (100), set the temperature limit to 20°C, and define the holding time. Press the START button and wait until the temperature limit is reached.

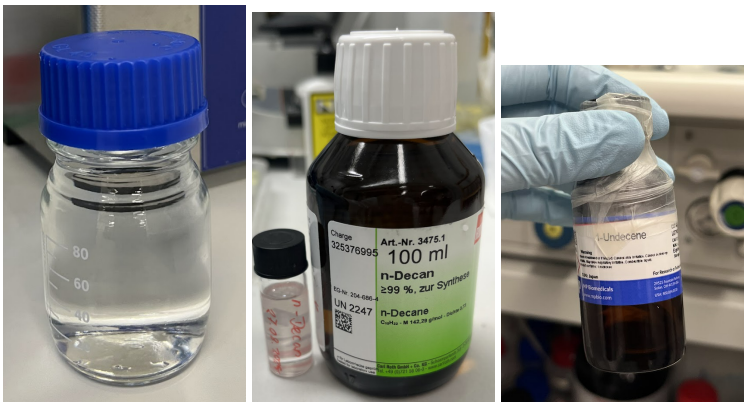


Figure 9: Tested liquids: (a) deionized water, (b) *n*-decane, (c) 1-undecene.



Figure 10: Elmasonic ultrasonic bath.

4. Verify that the gas inserts are properly locked into place.
5. Using the left hand, block the hole in the white plastic pump connector perpendicular to the purging tube. Simultaneously, pinch the narrow window tube to divert all nitrogen gas through the Purging Tube and Sample Chamber.
6. With nitrogen flowing through the Sample Chamber, block the gas outlet with the right hand for a few seconds to allow pressure to build, then release. Repeat for several minutes to complete the purging process. This procedure dilutes residual air inside the Sample Chamber with nitrogen gas by repeated pressurization and release.
7. Remove the two gas inserts and unblock the pump connector and window tube.
8. Switch the LNP95 to control the cooling speed according to the required sample temperature during the experiment.

3.3 Measurement

3.3.1 Measurement of the capillaries

1. Place the capillary sample over the aperture of the silver block and start the THMS600/720 Temperature-Controlled Stage (Linkam) and the Microscope (PRECiV Pro). Begin the experiment at ambient temperature (20°C), focusing on the meniscus of the liquid.

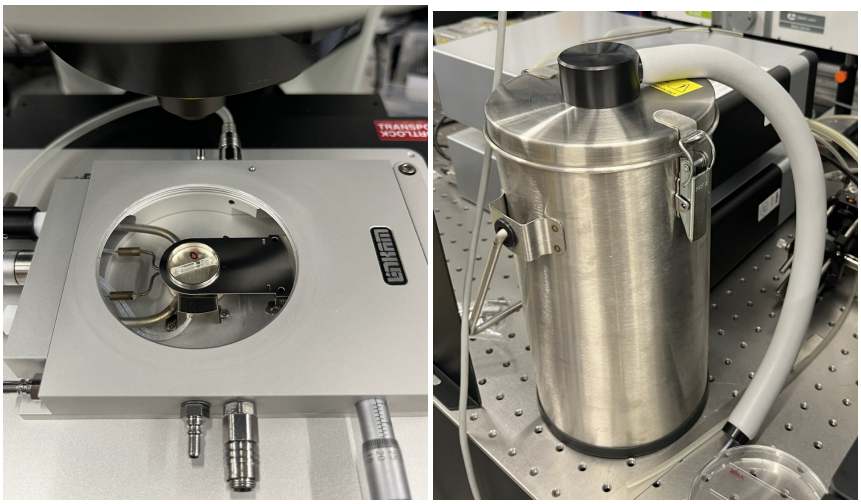


Figure 11: Temperature controlled stage: Linkam (left) and Liquid nitrogen (right).

2. Cool the liquid to a supercooled state at a high rate of approximately 20°C/min. Then, continue freezing at a lower rate of around 1°C/min until the liquid is fully solidified. Adjust the LNP95 cooling speed according to the freezing temperature of the liquid.

3. Adjust the z-axis to observe the formation of ice at the top of the capillary.

4. Heat the sample at a high rate until the premelting state begins, observing the partial transformation of solid to liquid.

5. Continue heating at a lower rate (around 1°C/min) until the meniscus reappears at the top of the capillary. Record this temperature as the melting point onset.

6. Continue heating at a low rate (around 1°C/min), increasing the temperature in 0.1°C increments until thermal equilibrium is reached. Adjust the z-axis to observe melting in other layers within the capillary.

7. Adjust the x- and y-axes to monitor the entire capillary until the sample is completely melted. Record this temperature as the melting point end.

3.3.2 Example of Melting Point Analysis with *n*-Dodecane

The melting and freezing behavior of *n*-Dodecane was investigated using the temperature-controlled stage. The onset temperature (where the first sign of phase change is observed) and the end temperature (where the transition is completed) were determined by direct optical inspection of the capillary content during heating and cooling.

1. At ambient temperature ($20\,^{\circ}$C), the sample remains in its liquid state. This temperature serves as the reference starting point.

2. Upon cooling, *n*-Dodecane remains liquid below its equilibrium freezing point, forming a supercooled liquid (see Fig. 12).

3. Further cooling leads to complete solidification of the liquid (see Fig. 13).

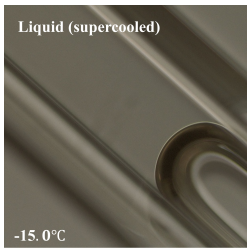


Figure 12: Supercooled liquid phase of *n*-Dodecane.

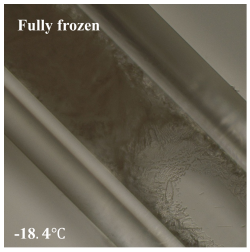


Figure 13: Fully frozen state of *n*-Dodecane.

4. The **onset temperature** is defined as the point at which the first nucleation event or crystalline structure is optically observed within the capillary.

5. During subsequent heating, the reverse transition (solid → liquid) was observed. The **onset melting temperature** was determined as the temperature at which the first region of liquid appeared, while the **end melting temperature** was defined as the point where the entire capillary content became liquid again. The **end temperature** corresponds to the point where the entire sample in the capillary appears fully crystalline, with no visible liquid phase remaining.

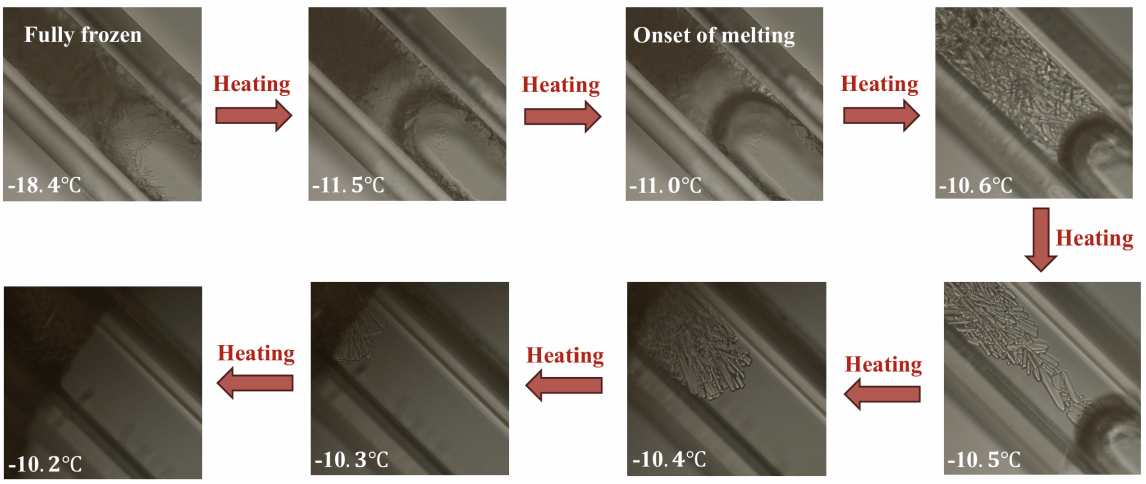


Figure 14: Phase transition of *n*-Dodecane during melting.

4 Results

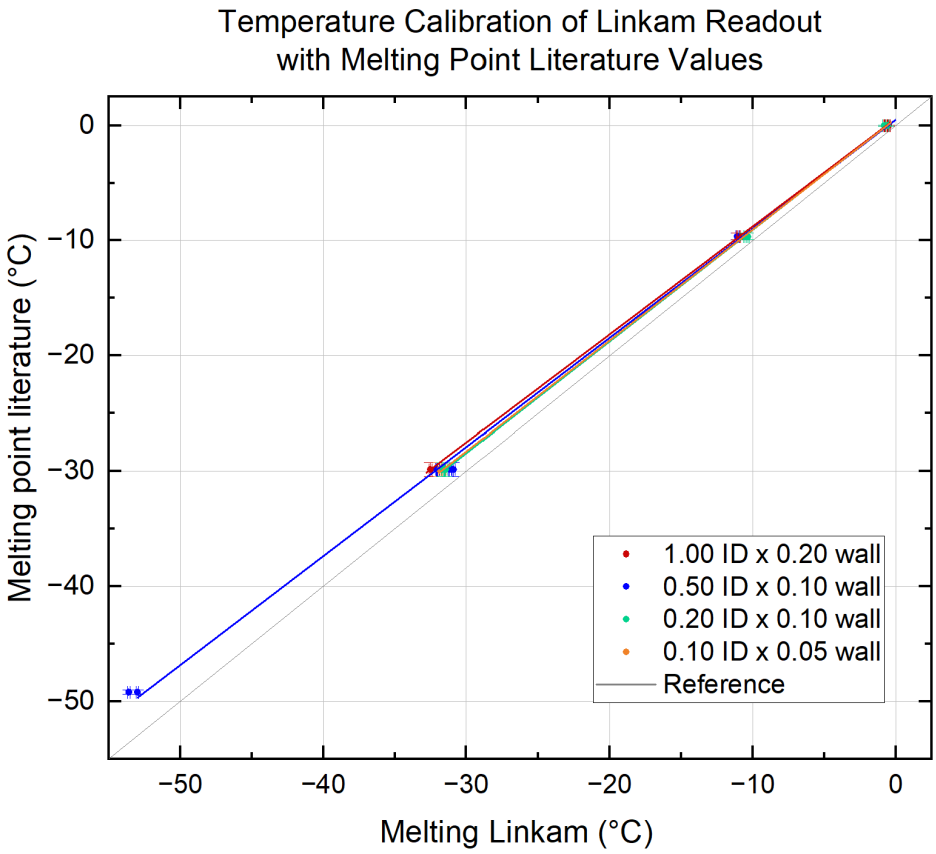


Figure 15: Calibration graph showing the relationship between Linkam stage temperature readout and the reference melting points for the investigated liquids.

The results of this study are presented as a temperature calibration graph in Figure 15, showing the relationship between the Linkam stage temperature readout and the reference melting points of the investigated liquids. Four different liquids with distinct melting points were studied: pure water, 1-undecane, n-decane, and n-dodecane. Each sample was confined within square glass capillaries of four diameters ($100\,\mu$m, $200\,\mu$m, $500\,\mu$m, and $1000\,\mu$m). All measurements were carried out using the same microscope setup that will later be employed for Raman spectroscopy measurements.

The melting point for each liquid was determined by cooling the sample until it was fully frozen, followed by controlled heating. The *onset of melting* was defined as the temperature at which the meniscus first reappeared, while the *end of melting* corresponded to the temperature at which the sample was fully melted across the aperture. The average melting temperature was calculated in Equation 1.

The measured melting points were compared to literature values: pure water (0.0°C), 1-undecane (-49.4°C), n-decane (-29.7°C), and n-dodecane (-9.6°C). These reference values form distinct distributions on the calibration graph. By relating the experimental melting points to the literature values, a linear calibration function was obtained:

$$T_{\text{real}} = a + b\,T_{\text{Linkam}}, \tag{2}$$

where T_{real} is the true melting temperature, T_{Linkam} is the Linkam stage readout, and the parameters a and b depend on the capillary size. Different linear relations were obtained for the four capillary diameters, and the fitted parameters are summarized in Table 2.

A comparison of experimental and reference values revealed a systematic deviation between the Linkam readout and the actual sample temperature. These deviations were dependent on the capillary diameter, with larger deviations observed in smaller capillaries. Ideally, if the Linkam readout directly reflected the true temperature of the confined liquid, all data points would align with the reference line (gray line, slope $= 1$). However, the experimental results consistently deviated from this line, highlighting the importance of temperature calibration for accurate interpretation of melting behavior in confined liquids.

Table 2: Fitted parameters a and b for the linear calibration progression in equation 2 calibration for different capillary sizes.

Capillary size	a	b
1.00 ID $\times$ 0.20 wall	-0.64485	1.06680
0.50 ID $\times$ 0.10 wall	-0.53506	1.05586
0.20 ID $\times$ 0.10 wall	-0.63386	1.03245
0.10 ID $\times$ 0.05 wall	-0.61329	1.03913

5 Conclusions and Outlook

Conclusions

In this report, I investigated the phase transition of various liquids (pure water, 1-undecane, n-decane, and n-dodecane) to study their melting points inside square capillaries with four different diameters (100 µm, 200 µm, 500 µm, and 1000 µm) using a Raman microscope.

The melting point was determined by first cooling the liquid until fully frozen, followed by controlled heating. The melting point onset was defined as the temperature at which the meniscus began to reappear, while the melting point end was defined as the temperature at which the sample was completely melted across the aperture.

From these experiments, I obtained a relationship between the melting points measured by the Linkam stage and the literature melting points (pure water: 0.0°C, 1-undecane: −49.4°C, n-decane: −29.7°C, n-dodecane: −9.6°C). The data showed a linear progression in equation 2.

Outlook

To improve the precision of the linear calibration, future work should include:

- Increasing the statistical reliability by repeating experiments for each capillary size.
- Extending the study to a wider temperature range by including substances with different melting points, such as dimethyl sulfoxide (DMSO, 18.5°C), n-undecane (−26.0°C), and isopropanol (−89.5°C).
- Investigating alternative capillary geometries (e.g., rectangular) and materials (e.g., fused silica) to evaluate their influence on phase transition behavior.

References

[1] Craig Landis. Strange scientific theory predicts a second type of liquid water, 2022. Accessed: 2025-09-10.

[2] Lars Gunnar Moody Pettersson, Richard Humfry Henchman, and Anders Nilsson. Water—the most anomalous liquid. *Chemical Reviews*, 116(13):7459–7462, 2016. PMID: 27405667.

[3] Vincent Holten and Mikhail A. Anisimov. Entropy-driven liquid–liquid separation in supercooled water. *Scientific Reports*, 2:713, 2012.

[4] Kenn E. Harding. Melting point range and phase diagrams- confusing laboratory textbook descriptions. *Journal of Chemical Education*, 76(2):224, 1999.

[5] C Cardelli, G Salvetti, and E Tombari. n-dodecane melting studied by the combined use of different calorimetric modes. *Thermochimica Acta*, 364(1):1–10, 2000.

[6] Sara Mosca, Claudia Conti, Nick Stone, and Pavel Matousek. Spatially offset raman spectroscopy. *Nature Reviews Methods Primers*, 1(1):21, 2021.

[7] Bruker. Raman spectrometer optics explained, 2025. Accessed: 2025-09-10.

[8] Pei-San Hung, Yichun Kuo, He-Guei Chen, Hui-Hua Chiang, and Oscar Lee. Detection of osteogenic differentiation by differential mineralized matrix production in mesenchymal stromal cells by raman spectroscopy. *PloS one*, 8:e65438, 05 2013.